Measuring the Nucleation Overpotential in Lithium Metal Batteries: Never Forget the Counter Electrode!

Journal of The Electrochemical Society, 2022 **169** 070509
1945-7111/2022/169(7)/070509/5/$40.00 © 2022 The Electrochemical Society ("ECS"). Published on behalf of ECS by IOP Publishing Limited

Measuring the Nucleation Overpotential in Lithium Metal Batteries: Never Forget the Counter Electrode!

Abdolkhaled Mohammadi,[1,2,3,z] Laure Monconduit,[1,3,4] Lorenzo Stievano,[1,3,4,z] and Reza Younesi[2,3]

[1]*ICGM, University Montpellier, CNRS, Montpellier, France*
[2]*Department of Chemistry, Ångström Laboratory, Uppsala University, 75121 Uppsala, Sweden*
[3]*Alistore-ERI, CNRS FR, Amiens, France*
[4]*RS2E, CNRS, Amiens, France*

The nucleation overpotential has been used by many researchers as an indicator of the energy required to form the Li nuclei during plating. Typically, a two-electrode system is used to measure the nucleation overpotential; this method, however, fails to show the contribution of working and counter electrodes separately. In this study, we have used a three-electrode configuration (three-dimensional nickel foam as working electrode, lithium foil as both reference and counter electrode) to deconvolute the potential associated with each electrode during the galvanostatic Li electrodeposition to obtain a clear picture of nucleation overpotential. The results indicate that, in such a system, the main source of overpotential is the sudden drop in the potential of the counter electrode, which can be attributed to the extraction of Li from the surface of lithium metal. Moreover, unlike the first half-cycle, the nuclear overpotential is dominated by the working electrode in the second half-discharge cycle, which should account for a true nucleation overpotential of the system. This finding may aid in clarifying the origins of the experimental polarization and preventing researchers from misinterpreting it in terms of nucleation overpotential.
 [DOI: 10.1149/1945-7111/ac7e73]

Manuscript submitted April 15, 2022; revised manuscript received June 14, 2022. Published July 13, 2022. *This paper is part of the JES Focus Issue on Nucleation and Growth: Measurements, Processes, and Materials.*

Supplementary material for this article is available online

Over the past four decades, many researchers have studied rechargeable Li metal batteries (LMBs) as a promising reversible energy storage system due to the high theoretical specific capacity and low electrochemical potential of the lithium metal negative electrode.[1] If the efforts to commercialize LMBs can be traced back to the mid-80s, those initial investigations had to come to a quick halt due to the safety issues and rapid capacity fading of LMBs.[2] A few successful attempts, such as Blue Car Bolloré cells with polymer-based electrolytes, have proved the applicability of such systems, in spite of some non-negligible drawbacks, such as the need of cycling above room temperature. Nevertheless, several major hurdles still subsist in the path of commercial use of LMBs with liquid electrolytes, namely their poor cycling lifetime, inadequate efficiency, and safety issues. The root of these problems lies in the dendritic growth of lithium during plating and the subsequent irregular dissolution of the dendrites, which leads to the formation of dead lithium which remains embedded in the growing solid electrolyte interphase (SEI), contributing to the extreme volume fluctuations.[3] A fundamental look into the Li deposition process can provide valuable insight into the working mechanism of LMBs and their shortcomings, thus paving the way to improving their performance and more widespread usage.[4–6] Despite considerable advancement in the understanding of the mechanisms involved in LMBs operation,[7–9] certain key issues are yet to be explored in-depth, especially the early-stage nucleation process of Li on different substrates.

In an LMB cell, the Li plating is normally initiated by heterogeneous nucleation of Li on the surface of the Li metal or other non-Li substrates.[10] The nucleation mechanism of the Li metal at the onset of the process is highly influential on the growth morphology of the plated Li and therefore can hold the key to inhibiting dendrite growth. The nucleation of a new solid phase needs to overcome a free energy barrier according to the classical nucleation theory.[11] In addition, the nucleation barrier for the electrodeposition of Li has been shown to be closely related to the nucleation overpotential. As shown in Fig. 1, at the beginning of the Li metal deposition process, a significant voltage drop is observed, followed by a flat voltage plateau. Visually, nucleation overpotential is represented by the difference between the voltage of the lowest point and the higher flat segment of the voltage plot. The nucleation overpotential indicates the energy required for the Li nucleation to take place; obviously, it has to be as low as possible.[11,12] The underlying mechanism of the nucleation overpotential is still considered a complex concept as it is affected by various factors including substrate properties, experimental conditions, electrolyte chemistry, and electric field distribution.[13]

To study the aforementioned parameter on lithium metal plating, a consistent part of the previous literature includes galvanostatic cycling and/or polarization test experiments that are performed using cells in a two-electrode configuration with a piece of lithium foil as the counter electrode. In most such studies, any measured overpotential tends to be attributed principally to the properties of the working electrode, which assumes that the lithium counter electrode works as an "ideal" counter/reference electrode with no contribution to the measured potential. However, such an assumption may lead to misleading conclusions since the lithium counter/reference electrode may indeed also substantially contribute to the overall observed overpotential. To gain more insight into the electrochemical reactions and voltage changes, a three-electrode set-up should be used whereby each individual electrode's contribution to the overall behavior of the system is studied independently.[14,15]

In this work, to address the impact of the Li counter electrode on the nucleation overpotential peak, we deconvoluted each source of electrode polarization during galvanostatic Li electrodeposition at various conditions including different electrolytes, Li surface, and current densities. Our results reveal that the initial drop in cell voltage, in some literature cases attributed to the nucleation overpotential during plating on the working electrode, is rather dependent upon the potential of the Li counter electrode, where lithium stripping from the Li metal surface needs to be activated. This study can help unfolding the origin of the nucleation overpotential, preventing researchers from overlooking the nucleation overpotential as an indicator for the energy required to initiate Li nucleation.

Results and Discussion

The variation in voltage during cell cycling has been often used to gain insight into the mechanisms behind Li nucleation,

[z]E-mail: Abdolkhaled.mohammadi@umontpellier.fr; Lorenzo.stievano@umontpellier.fr

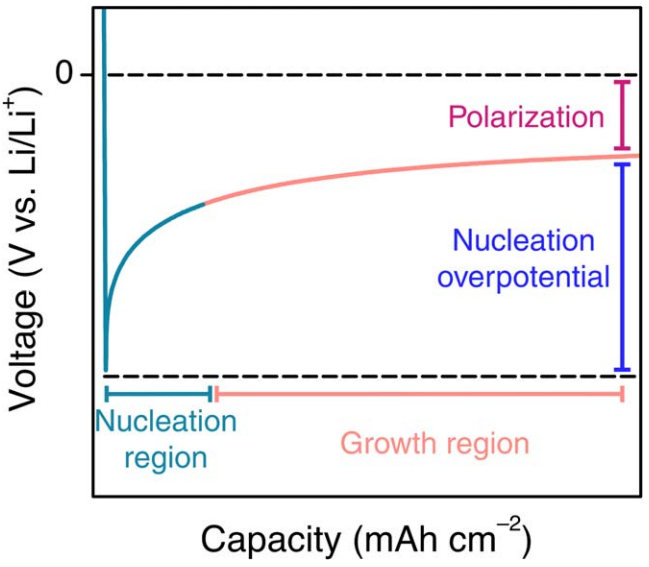

Figure 1. Schematic plot of the typical voltage profiles of galvanostatic Li deposition.

dissolution, and deposition.[8,16–18] Figure 2a shows the overall voltage trace ($E_{working}$-$E_{counter}$) measured in a three-electrode cell containing a Ni foam working electrode and a Li counter electrode during the first lithium plating process. In this process, the cell voltage reaches a minimum before rising to the higher flat segment of the potential. Such a trace can be divided into three separate stages, which will be discussed in detail hereafter.

Figure 2b shows the evolution of the voltages of the individual Ni foam working electrode ($E_{working}$, blue) and a Li counter electrode ($E_{counter}$, red), as well as the overall voltage profile ($E_{working}$-$E_{counter}$, black) of the same system during one and a half galvanostatic cycles. In such a three-electrode configuration, indeed, one can observe the electrochemical behavior of each electrode separately and arrive at a more comprehensive understanding of the overall voltage variations. Since cell configuration has a strong influence on the electrochemical performance of the batteries,[19,20] two-electrode coin cell tests were performed in parallel under the same condition to determine if they had any effect on the voltage variation. It must be underlined that two-electrode coin cell tests showed very similar voltage profiles to those obtained in three-electrode setups, which implies that in both cases the voltage behavior is governed by similar phenomena (cf Fig. S1 (available online at stacks.iop.org/JES/169/070509/mmedia)).

Stage I (Earliest stage).—After resting time and when a current is applied to the cell, the potential of the working electrode ($E_{working}$) drops immediately from 2.7 to 1.2 V (Fig. 2a), and conversely, on the Li electrode the potential increases from about 0.01 to 0.25 V (Fig. 2b). The change in potential of the working electrode is more significant than that of the counter electrode. Consequently, a drop of potential in the working electrode dominates the overall voltage profile ($E_{working}$-$E_{counter} \approx E_{working}$). The potential increase of the lithium metal counter electrode in the first cycle is due to the surface contamination/passivation of the Li metal. The pristine Li surface forms a non-homogenous native surface layer containing compounds such as nitrides, LiOH, Li_2O, and Li_2CO_3, which is formed during manufacturing and storage in gloveboxes, and a chemical SEI layer with organic and inorganic species resulting from the contact with the electrolyte.[21–23] In order to break this passivation layer, the Li electrode's overpotential has to increase at the beginning of the application of the current. Hence, the higher overpotential means that the Li surface is relatively more passivated. In order to verify whether a change in surface chemistry causes a change in this potential hike, electrolyte type and Li surface modification were investigated. As shown in Fig. S2c, the initial potential of Li metal anode in carbonate-based (1.0 M $LiPF_6$ in EC/DMC (1/1 w/w), LP30) electrolytes is higher than that of ether-based (1.0 M LiTFSI in DOL/DME (1/1 vol.) + 2% of $LiNO_3$) electrolytes due to the less compatibility between Li metals and carbonate-based solvents. In addition, an artificial SEI formed by a mixture of Li_7Sn_2 and LiCl was formed on the surface of Li through by surface treatment with $SnCl_2$ (as detailed in one of our previous works).[24] Such artificial SEI coatings are known to favor ion transportation and consequently improve the interface stability over battery cycles. As shown in Fig. S3, modification of the Li surface leads to a decrease in the initial potential rise at the counter electrode, which confirms that the initial increase in the potential of the counter electrode is highly dependent on the surface chemistry and conditions of Li metal.

Stage II (SEI formation).—After the cell is discharged to 0.2 V, the potentials of both working and counter electrode steadily and rapidly decreases. The SEI layer formation takes place on the working electrode while Li reacts with impurities or native oxides layer on the surface of the working electrode. Due to the small amount of oxide layer and the rapid formation of the SEI, the working electrode potential reduction occurs rapidly; meanwhile, the overall potential is the same as the working electrode from about 1.2 to 0.2 V ($E_{working}$-$E_{counter} \approx E_{working}$).

Stage III (Nucleation overpotential).—As the discharge process continues ($E_{working}$-$E_{counter} < 0$ V), the voltage suddenly drops at some point and then remains stable on a plateau. The difference between the lowest point of the voltage drops and the later flat level is known as the nucleation overpotential (Fig. 2b), which has been suggested to be influenced by the energy required to form the Li nuclei on the surface of non-Li substrates or Li metal.[11,12] Therefore, a lower nucleation overpotential means Li faces a weaker barrier for nucleation and deposition. Moreover, the nucleation overpotential is considered a significant parameter in measuring the lithiophilicity of the modified non-Li substrate.[25–27] Based on the previous reports, the initial Li nucleation overpotential is quite high for the

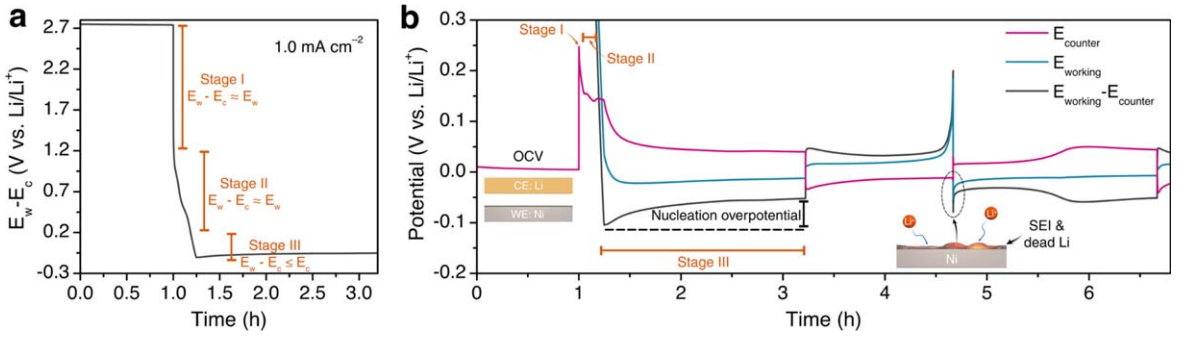

Figure 2. (a) the electrochemical potential curve for half-cycle electrodeposition of Li, and (b) Potential profiles of the electrodes and the cell during plating and stripping in a Swagelok three-electrode cell at 1.0 mA cm^{-2} current density in 1 M LiTFSI DOL/DME, 2% $LiNO_3$ electrolyte.

conventional substrates such as Ni or Cu foam, since these materials have little affinity for Li.[13,28] By contrast, this study shows that the overpotential at the Li counter electrode can mainly explain the initial decrease in voltage of the cell below 0.2 V. On the Ni foam, there is a constant voltage decrease to a steady-state level, which indicates that the energy barrier for extracting Li on the surface of Li is much higher compared to the energy barrier for forming nucleation sites ($E_{working}$-$E_{counter} < E_{counter}$). Once the nucleation overpotential is overcome, the system experiences a gradual decrease in the overall potential during the Li deposition process until a stable state is reached. Furthermore, by comparing the working overpotential in carbonate-based (LP30) with ether-based electrolytes (Fig. S2b), a small peak appears in the working potential for the LP30. This indicates that in nucleation peak on the working electrode depends on the electrolyte species and the SEI formed on the surface. Overall, in both electrolytes, the Li counter electrode rather than the Ni foam working electrode is the predominant source of the system's overpotentials and modification of the voltage curve.

Following stages.—During the stripping process of the Li plated on the Ni foam, it is also quite evident that the Li counter electrode is responsible for the voltage increase since the Li nucleation and the SEI layer on the Li metal electrode oppose a certain resistance, while little energy is needed to strip Li from the dendrites plated on the Ni foam surface.[8] At the end of this process, once the active Li is completely consumed, a sharp increase in voltage is observed. The SEM images show that residual SEI and inactive (dead) Li (Fig S4) cover the surface of Ni foam at the end of the stripping process. This is most likely the reason why, at the very beginning of the second Li plating process, the cell undergoes an overall voltage decrease due to the drop in potential at the Ni foam electrode. This could explain why the second cycle for the working electrode has a higher nucleation overpotential compared to the first cycle. Also, in accordance with the previous experiment results,[16] the shape of the potential profile of the counter electrode changes during the second plating process in a manner that is highly similar to that of the coin cell (Fig. S1). As previously reported,[8,18] the first plateau corresponds to the stripping of Li from the pre-existing mossy dendrites on the surface of the Li. After no lithium is left to be extracted from the dendritic surface, the overpotential starts to increase due to the Li stripping from the bulk Li anode electrode.[8] As shown in Fig. S5, later cycles show a similar Li deposition/dissolution pattern and include SEI fracture, fresh Li nucleation, dendrite growth, and dead Li formation at both ends.

The applied current density has a significant impact on the electrodeposition behavior and overpotential of the cell in LMBs.[29] To examine the effect of current density on the nucleation overpotential, the plating/stripping current density was varied between 0.2 and 2.0 mA cm^{-2} (Figs. 3, 4). For the first cycle, the results show that reducing the current density leads to a lower overpotential for the overall cell voltage and a dominant contribution always coming from the lithium counter electrode (Figs. 3b, 3c, and 4), i.e., from the stripping at the counter electrode. Indeed, the potential peaks marked by arrows in Fig. 3c correspond to the nucleation peaks in the overall cell-voltage profile (Fig. 3a) and are thus a consequence of Li extracting from the counter electrode. It should be noted that, as the current density decreases, the stripping peaks in the counter electrode (shown by arrows in Fig. 3c) shift to the right. The extra amount of charge required at lower current densities for the formation of the SEI layer is responsible for Li stripping peaks shifts.[11] Furthermore, the slight increase and decrease of the potential plateau values of the working and counter electrodes, respectively, when the current density is reduced from 2.0 to 0.2 mA cm^{-2}, reflect possible slight differences in the Li^+ concentration gradient at the electrode surfaces and of the simple ohmic contribution to the overpotential.[11,13] On decreasing the current, even though the contribution of the working electrode to the nucleation overpotential increases, that of the Li counter electrode remains dominant.

The different contributions to the overpotential obtained from the second plating process at increasing current densities can be derived from the profiling potentials shown in Figs. 3d–3f for the full cell, the working and the counter electrode, respectively. The zoomed-in insets of plots (e) and (f) show that, unlike the first plating process, even though the counter electrode contribution is not zero, the nucleation overpotential is this time dominated by the working electrode. As shown at the bottom of Fig. 4, three independent measurements were used to evaluate the average potential contribution of the working and counter electrodes to the overall cell

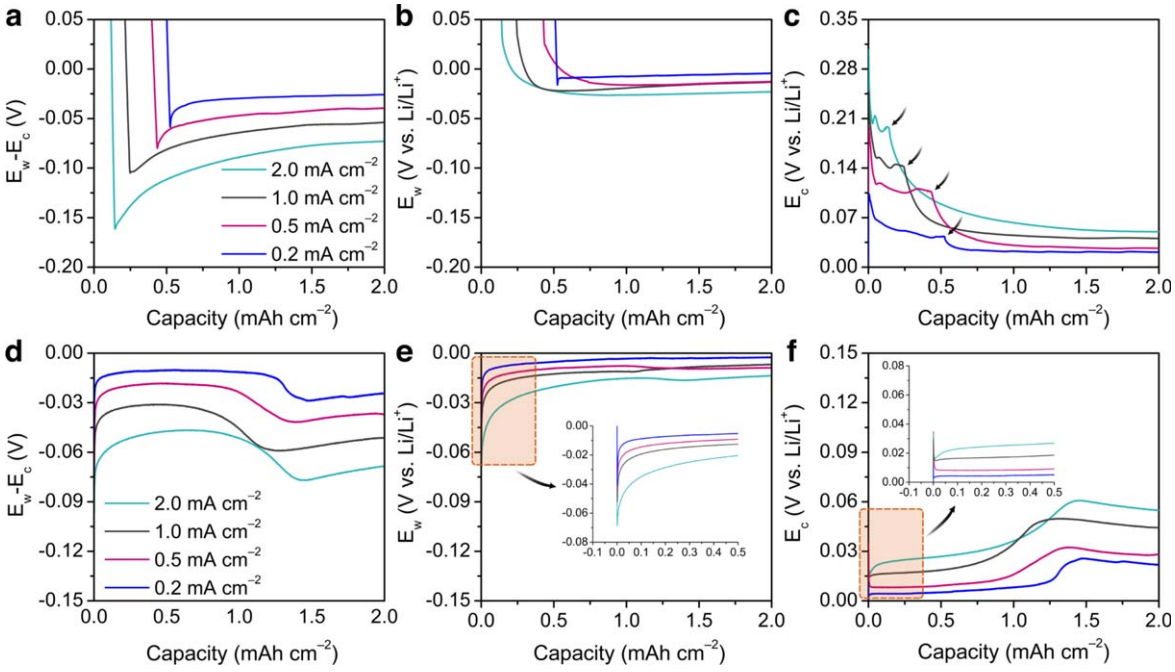

Figure 3. The plating process profile in Swagelok three-electrode system for the 1st (a)–(c) and 2nd (d)–(f) cycle at different current densities and the corresponding potential variation of the: (a), (d) overall cell-voltage profile, (b), (e) working, and (c), (f) counter electrode in 1 M LiTFSI DOL/DME, 2% $LiNO_3$ electrolyte (The insets of Figs. e and f show the highlighted zoomed-in area).

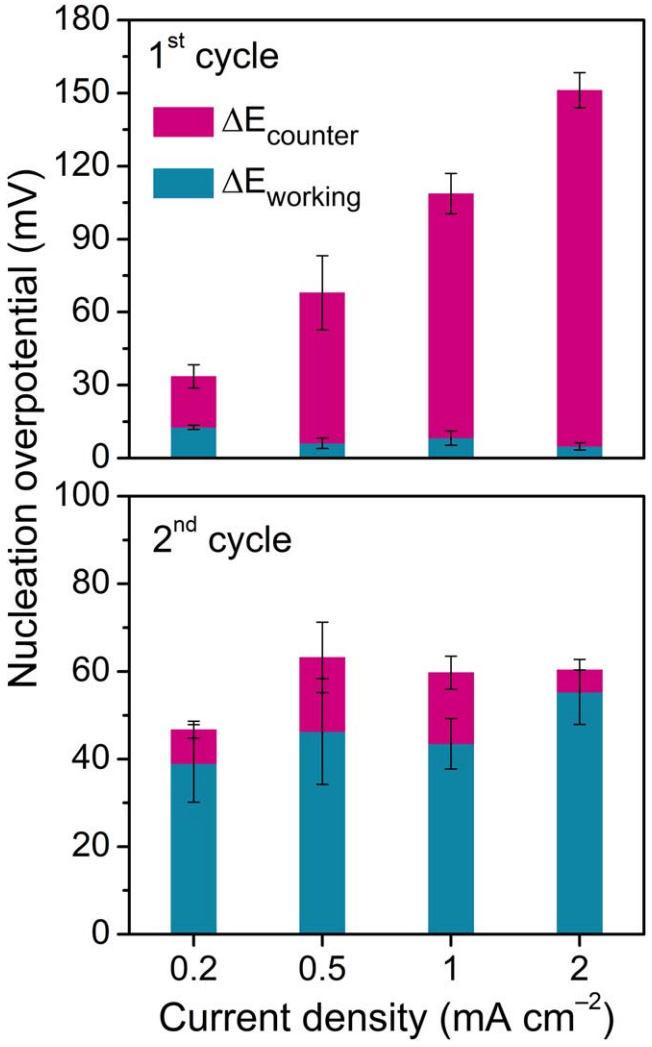

Figure 4. Potential contribution of the working and counter electrodes to the overall cell nucleation overpotential for the 1st (top) and 2nd (bottom) cycles in 1 M LiTFSI DOL/DME, 2% $LiNO_3$ electrolyte (The error bars represent the standard deviation, obtained from three independent Swagelok three-electrode replicates).

nucleation overpotential for the 2nd cycle. From these results, it is obvious that the working electrode has a dominant impact on the nucleation overpotential compared to the counter electrode only for the second cycle,. For the first cycle, on the other hand, the contribution of the counter electrode is largely predominant in the overall cell nucleation overpotential. Concerning the evolution of the overpotential value, its increase in the first cycle is clearly connected to the increase of the stripping overpotential, whereas its timid growth in the second cycle can be mostly related to the effective nucleation overpotential (within the experimental error). This observation suggests that a better estimate of the nucleation overpotential in two-electrode cells should be derived from the second plating/stripping cycle rather than from the first one. Besides, the modification of the counter electrode's potential in the second part of the second plating process is responsible for the drastic change in the cell potential (Fig. 3f). As mentioned in the introduction and already widely reported in the literature, this effect can be correlated to the incomplete stripping of the previously plated dendrites at the counter electrode, and the inset of lithium stripping from the bulk of the lithium counter electrode.[8,16,18] Based on these observations, to ensure a more accurate interpretation of the data, we recommend the use of a three-electrode configuration[15,30] to correctly evaluate the nucleation overpotential of the Li metal system, or at least to focus on the second plating process (or the following ones) in the case of the use of a two-electrode cell.

Conclusions

The importance of using a three-electrode cell configuration to study voltage profiles during lithium plating/stripping cycling experiments is here discussed. During the Li plating process, the potential of the working electrode shows a very small nucleation overpotential for the electrolyte/electrode system studied here, indicating that the main part of the cell overpotential originates from the Li-metal counter electrode. The stripping or extraction of Li from the lithium metal counter electrode during the first plating process at the working electrode requires overcoming a bigger energy barrier in contrast to the energy needed for forming the nucleation sites on the working electrode. At low current densities, even though the contribution of the working electrode decreases, the lithium metal counter electrode has still the biggest influence on the nucleation overpotential. The results show that from the second cycle, however, the nucleation overpotential can be more safely estimated from the working electrode. The outcome of this work highlights that the results and interoperation from two-electrode setups using Li metal counter electrode can be misleading, and that the use of a three-electrode cell with a reference electrode should be preferred.

Acknowledgments

The Alistore-European Research Institute (ALISTORE-ERI) network is warmly thanked for funding the PhD grant of A. M. The authors gratefully acknowledge financial support from the French National Research Agency (project Labex STORE-EX, ANR-10-LABX-76–01).

ORCID

Abdolkhaled Mohammadi https://orcid.org/0000-0002-7936-3407
Laure Monconduit https://orcid.org/0000-0003-3698-856X
Lorenzo Stievano https://orcid.org/0000-0001-8548-0231
Reza Younesi https://orcid.org/0000-0003-2538-8104

References

1. X. He et al., *Nat. Rev. Mater.*, **6**, 1036 (2021).
2. X. B. Cheng, R. Zhang, C. Z. Zhao, and Q. Zhang, *Chem. Rev.*, **117**, 10403 (2017).
3. D. Lin, Y. Liu, and Y. Cui, *Nat. Nanotechnol.*, **12**, 194 (2017).
4. B. Horstmann et al., *Energy Environ. Sci.*, **14**, 5289 (2021).
5. Z. Wang, Z. Sun, J. Li, Y. Shi, C. Sun, B. An, H. M. Cheng, and F. Li, *Chem. Soc. Rev.*, **50**, 3178 (2021).
6. J. Touja, N. Louvain, L. Stievano, L. Monconduit, and R. Berthelot, *Batter. Supercaps*, **4**, 1252 (2021).
7. F. Liu et al., *Nature*, **600**, 659 (2021).
8. K. N. Wood, E. Kazyak, A. F. Chadwick, K.-H. Chen, J.-G. Zhang, K. Thornton, and N. P. Dasgupta, *ACS Cent. Sci.*, **2**, 790 (2016).
9. J. Betz, J. P. Brinkmann, R. Nölle, C. Lürenbaum, M. Kolek, M. C. Stan, M. Winter, and T. Placke, *Adv. Energy Mater.*, **9**, 1 (2019).
10. A. J. Sanchez, E. Kazyak, Y. Chen, K. H. Chen, E. R. Pattison, and N. P. Dasgupta, *ACS Energy Lett.*, **5**, 994 (2020).
11. A. Pei, G. Zheng, F. Shi, Y. Li, and Y. Cui, *Nano Lett.*, **17**, 1132 (2017).
12. P. Biswal, S. Stalin, A. Kludze, S. Choudhury, and L. A. Archer, *Nano Lett.*, **19**, 8191 (2019).
13. P. Zou, Y. Sui, H. Zhan, C. Wang, H. L. Xin, H. M. Cheng, F. Kang, and C. Yang, *Chem. Rev.*, **121**, 5986 (2021).
14. R. Dugas, J. D. Forero-Saboya, and A. Ponrouch, *Chem. Mater.*, **31**, 8613 (2019).
15. R. Nölle, K. Beltrop, F. Holtstiege, J. Kasnatscheew, T. Placke, and M. Winter, *Mater. Today*, **32**, 131 (2020).
16. C. J. Huang et al., *Nat. Commun.*, **12**, 1 (2021).
17. K. H. Chen, K. N. Wood, E. Kazyak, W. S. Lepage, A. L. Davis, A. J. Sanchez, and N. P. Dasgupta, *J. Mater. Chem. A*, **5**, 11671 (2017).
18. G. Bieker, M. Winter, and P. Bieker, *Phys. Chem. Chem. Phys.*, **17**, 8670 (2015).
19. Y. Xiao, R. Xu, C. Yan, J. Q. Huang, Q. Zhang, and M. Ouyang, *Adv. Funct. Mater.*, **32**, 2108449 (2022).
20. R. Raccichini, M. Amores, and G. Hinds, *Batteries*, **5**, 1 (2019).
21. K. Kanamura, H. Tamura, and Z. ichiro Takehara, *J. Electroanal. Chem.*, **333**, 127 (1992).
22. R. Younesi, G. M. Veith, P. Johansson, K. Edström, and T. Vegge, *Energy Environ. Sci.*, **8**, 1905 (2015).

23. R. Younesi and F. Bardé, *Sci Rep.*, **7**, 3 (2017).
24. A. Hagopian, J. Touja, N. Louvain, L. Stievano, J. S. Filhol, and L. Monconduit, *ACS Appl. Mater. Interfaces*, **14**, 10319 (2022).
25. J. Park, S. Ha, J. Y. Jung, J. Hyun, S. Yu, H. Lim, N. D. Kim, and Y. S. Yun, *Adv. Sci.*, **9**, 2104145 (2021).
26. F. Hu, Z. Li, S. Wang, and W. E. Tenhaeff, *ACS Appl. Mater. Interfaces*, **12**, 39674 (2020).
27. J. Yun, E. S. Won, H. S. Shin, K. N. Jung, and J. W. Lee, *J. Mater. Chem. A*, **7**, 23208 (2019).
28. S. Park, H. J. Jin, and Y. S. Yun, *Adv. Mater.*, **32**, 2002193 (2020).
29. H. Kühnle, E. Knobbe, and E. Figgemeier, *J. Electrochem. Soc.*, **169**, 040528 (2022).
30. K. Yan, Z. Lu, H. W. Lee, F. Xiong, P. C. Hsu, Y. Li, J. Zhao, S. Chu, and Y. Cui, *Nat. Energy*, **1**, 16010 (2016).